Final Progress Report

1. DOE Grant Number DE-FG02-07ER46447; Vanderbilt University, Nashville, TN

2. *Structure and Magnetic Properties of Lanthanide Nanocrystals*
Principal Investigator: Dr. James H. Dickerson

3. Submission: June 1, 2014; Period Covered: August 1, 2007-August 15, 2011

4. Description of Accomplishments:

We have had considerable success on this project, particularly in the understanding of the relationship between nanostructure and magnetic properties in lanthanide nanocrystals. We also have successfully facilitated the doctoral degrees of Dr. Suseela Somarajan, in the Department of Physics and Astronomy, and Dr. Melissa Harrison, in the Materials Science Program. The following passages summarize the various accomplishments that were featured in 9 publications that were generated based on support from this grant. We thank the Department of Energy for their generous support of our research efforts in this area of materials science, magnetism, and electron microscopy.

A. Synthesis of Sub-2.0 nm EuS Nanocrystals:

The thermal decomposition of single molecular precursors has been proven to be an effective method to synthesize nanoscale metallic chalcogenides.[1] Finer control over these parameters can be obtained using different precursors and a refined thermolysis. Our technique to produce sub-2.0 nm EuS nanoparticles involves a thermolysis procedure of a synthesized single-source precursor, a method similar to that observed by others.[2-4] For the preparation of single source Eu precursor, we used a procedure similar to that reported for the synthesis of heteroligand lanthanide(III) diethyldithiocarbamate complexes with phenanthroline.[5-7] The decomposition procedure of the EuS nanoparticles was pursued via thermogravimetric analysis (TGA) and derivative thermogravimetric (DTG) analysis. A 1 mM methanolic solution of 1,10-phenanthroline was added under vigorous stirring to a 1 mM methanolic solution of $EuCl_2$. Thereafter, 2 mM of diethylammonium diethyldithiocarbamate were added into the reaction mixture, producing an orange precipitate. The orange EuS precursor crystals were isolated by centrifugation, washed twice with methanol and dried under vacuum. This work demonstrates that the synthesized resultant heteroligand complexes display high stability against hydrolysis, which tends to be the main obstacle for the successful fabrication of europium chalcogenides.[8-10]

For the synthesis of EuS nanoparticles, we transferred the precursor to a porcelain boat and inserted it into a horizontal tube furnace (Thermolyne #F21135, Barnstead International) for a time-sensitive mass reduction step. A steady stream of dry, ultrapure nitrogen prevented unintended hydrolysis or unintended devolution of the precursors. We heated the materials for approximately one hour at 700 ºC. After this step, the resultant solid was cooled gradually to room temperature. Adjustments of

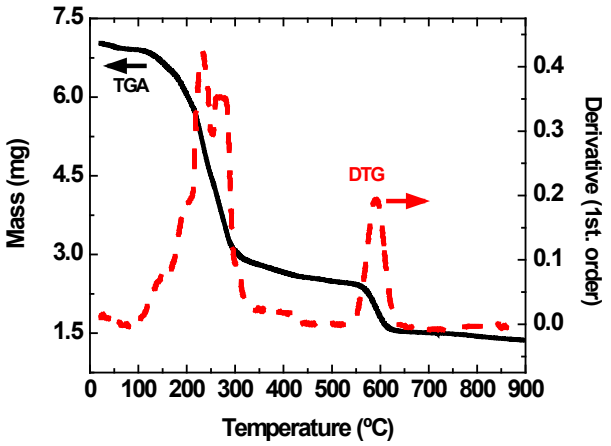

Fig. 1: TGA (solid line) and DTG (dashed line) analysis of the EuS precursor.

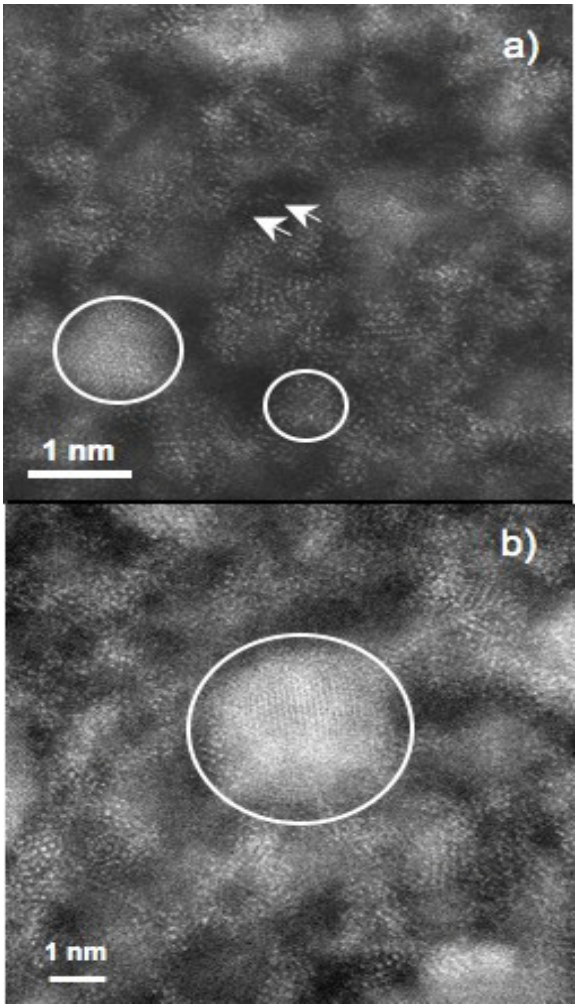

Fig. 2: Two HAADF images of EuS nanoparticles with bright intensities representing Eu atoms. (a) A (1.10 ± 0.20) nm nanoparticle neighboring one with a nominal diameter of (0.72 ± 0.13) nm. (b) A larger, (3.70 ± 0.67) nm nanoparticle. Each of the aforementioned nanoparticles is encircled to guide the eye. The positions of isolated single Eu atoms are indicated by arrows.

decomposition temperature and time, and ramp-up/ramp-down time, yielded dispersed nanocrystalline particles with controllable size. This produces nanoparticles, which were dispersed in a variety of manners. For our studies, we dispersed the EuS nanocrystalline powder in an oleic acid solution or 2,2'-bipyridyl (Alfa Aesar).

To assess the suitability of the precursor, prepared as described above for EuS nanoparticle synthesis, TGA was performed across a temperature range from 25 ºC up to 900 ºC at a heating rate of 10 ºC min^{-1} under nitrogen atmosphere. The starting precursor mass for the analyses was 7 mg. The resulting TGA and DTG curves, which characterize the thermal decomposition of the precurosrs, are presented in Figure 1. The EuS precursor decomposes in two steps. The majority of the mass loss, approximately 50 %, occured in the 100 ºC to 350 ºC temperature region. This corresponds to pronounced peaks in the DTG curve at 200 ºC and 232 ºC, which indicates the rapid, vigorous decomposition of the single source precursor and the initial nucleation and growth of the EuS nanoparticles. Another smaller transition in the TGA designated a second stage in the decomposition process. This occurred in the 500 ºC to 625 ºC temperature range. The corresponding DTG curve displayed the maximum decomposition rate at 588 ºC with a mass loss of 12.5 % during this transition. It represented the decomposition of residual inorganic and organic compounds of the initial precursor material, yielding the final product at the end of decomposition: EuS NCs. The final residual mass was twenty-five percent of the original. At the high temperature of 700 ºC chosen for our synthesis, fast nucleation and growth of EuS is anticipated to promote the formation of ultrasmall particles.

B. Electron microscopy of sub-2.0nm EuS nanocrystals:

For our analysis of the size and structure of the nanomaterials, methanolic solutions of the EuS nanoparticles were dropcasted onto holey carbon films mounted on TEM specimen grids (Ted Pella, Inc.). High-angle annular dark-field (HAADF) Z-contrast scanning transmission electron microscopy (Z-STEM) images were acquired using an aberration-corrected VG Microscope HB603 U STEM, which was operated at 300 KeV.[11] Electron probe diameters were below 0.1 nm. Electron beam currents of less than 20 pA and dwell times of 32 µs/pixel were used.

Figure 2 shows two representative HAADF images of the EuS nanoparticles with bright image intensities representing Eu atoms. The chosen imaging conditions limit the visibility of sulfur and carbon atoms due to the large difference in the atomic numbers for Eu (Z=63), S (Z=16) and C (Z=6). The STEM analysis revelead highly crystalline face-centered cubic nanoparticles (encircled), the

majority of which has dimensions well below 2 nm. For example, in Figure 2a two nanoparticles with nominal diameters of (1.10 ± 0.20) nm and (0.72 ± 0.13) nm are encircled. The detection of isolated Eu atoms dispersed on the carbon support film (marked by arrows) indicates atomic resolution and single atom sensitivity during the STEM experiments. In many areas of the sample, non-crystalline agglomerates of Eu atoms (likely in conjunction with sulfur atoms) were observed. More detailed investigations of the crystallinity of the EuS nanoparticles and their lattice plane spacings requires selected area electron diffraction experiments, which will be subject of future work. However, for the *quantum-confined*, sub-2.0 nm EuS nanomaterials, HAADF data provide both direct evidence for the size and crystallinity of the nanoparticles, and first indications of size-induced structural re-arrangements within individual particles.

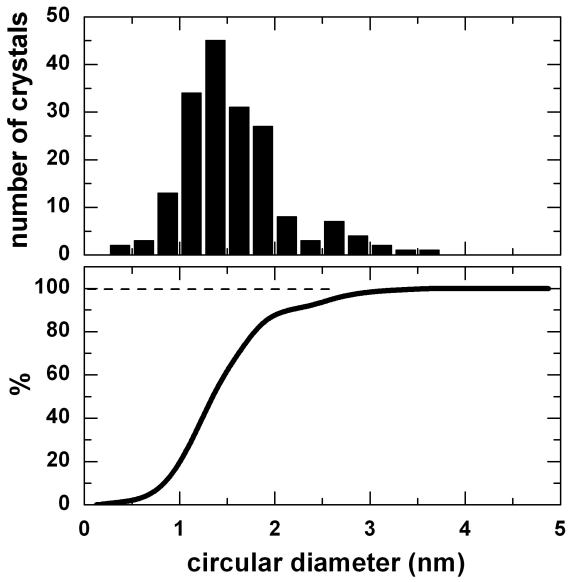

Fig. 3: a) Histogram of the EuS nanoparticle sizes prepared by thermolysis at 700 ºC as a function of circular diameter (see text). b) Percentage of the synthesized nanomaterials whose size are smaller than or equal to the corresponding circular diameter.

A plot of the EuS nanoparticle size distribution is provided in Figure 3a. The abcissa label, circular particle diameter, refers to the diameter of a sphere characterized by the same area as covered by the individual particles. Thus, the diameter of the nanoparticles observed in the HAADF images were distributed in Figure 3a under the corresponding circular diameter. All reported circular diameters in Figure 3 are subject to an uncertainty of 18 %. Approximately 45 % of the analyzed nanoparticles have circular diameters between 1.25 nm and 1.5 nm. Additional statistics, provided in Figure 3b, reveal that 88 % of the particles are characterized by diameters below 2.0 nm. Therefore, the predominance of the nanomaterials synthesized according to the reported methods reside within the ultrasmall, quantum-confined regime.

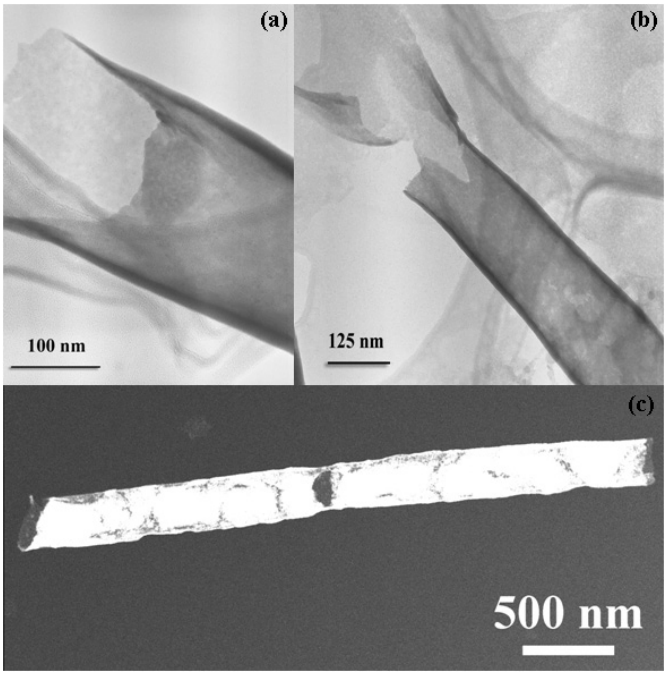

Fig. 4: (a) and (b) transmission electron microscope images of EuS nanotubes. (c) scanning transmission electron microscope image of a EuS nanotube.

EuS nanoparticles with sub-2 nm sizes were synthesized by a thermolysis of a single source precursor —europium diethyldithiocarbamate complex with 1,10-phenanthroline. Favorable synthetic conditions for EuS nanomaterials with the sizes well below 2 nm were studied by TGA and DTA analysis and confirmed by direct imaging using aberration corrected STEM. We plan to continue our investigation of the relationship between the magnetic properties, the atomic arrangement, and the size of these lanthanide chalcogenide nanomaterials.

B. First Synthesis and Characterization of EuS Nanotubes:

Our interest in europium sulfide (EuS) nanotubes stems from our interest in how shape anisotropy in nanostructures can give rise to changes in the local crystallinity of the material. These deformations in the crystallinity can induce modifications in the physical properties (optical, magnetic, etc.) of the nanostructures. For commercial applications, this pursuit is motivated by the possible realization of novel magneto-optical materials that could be employed for optical switching, waveguides, and optical isolation in telecommunications and optical computing applications. In our study of EuS nanotubes, we employed a single-source molecular precursor, as described in previous reports of the synthesis of EuS nanocrystals[12]. Anopore™ inorganic membranes (Anodisc™; Whatman, Inc.), composed of amorphous alumina, were used for the template-assisted synthesis of the EuS nanotubes. A 15 mM, chloroformic solution of the single source precursor was added dropwise into the pores of the alumina membranes. Next, the saturated alumina membranes were transferred to a horizontal tube furnace for thermolysis in a nitrogen environment at 350ºC for 12 hours. During this step, the precursor thermally decomposes to form anisotropic EuS nanostructures. Following thermolysis, the alumina membranes were dissolved in a 0.25 M solution of NaOH. Once the membrane is dissolved, the nanotubes were dispersed in methanol and centrifuged for 45 minutes at 10,000 rpm for cleaning.

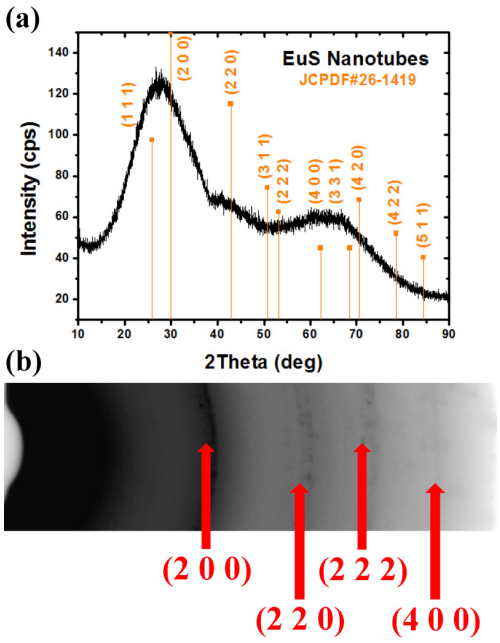

Fig. 5. (a) XRD spectrum revealing the primary, secondary, and tertiary diffraction peaks for fcc EuS: (2 0 0), (1 1 1) and (2 2 0). **(b)** Inverted SAED spectrum of EuS nanotubes giving evidence of the fcc EuS crystallinity. The SAED ring pattern also includes diffraction rings, in which, the corresponding d-spacings deviate from that of unstrained bulk fcc EuS.

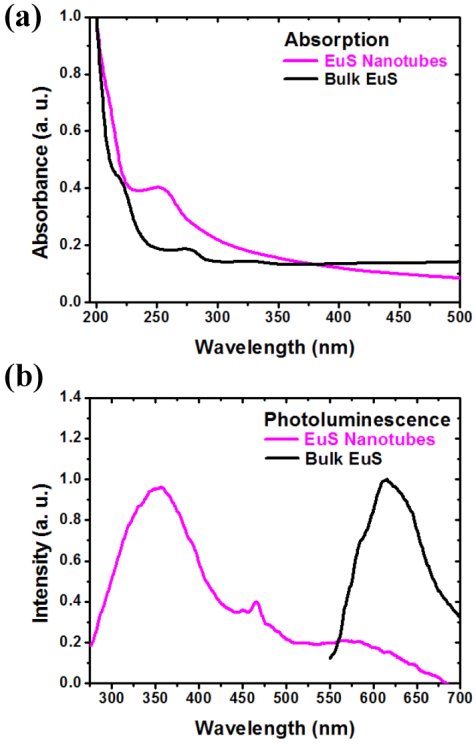

Fig. 6. Room temperature, blue-shifted optical properties of the EuS nanotubes samples can be seen in the normalized **(a)** absorption and **(b)** photoluminescence spectra. The observed, absorption and luminescence of the EuS nanotubes samples is due to quantum confinement, in conjunction with strain-induced effects.

The wall thicknesses of the EuS nanotubes are estimated to be 2-5 nm. Annular dark field, scanning transmission electron microscopy (STEM) images were taken using a JEOL JEM 2500SE operated at 200 kV. Analysis of the structures via STEM confirmed that the EuS nanotubes are polycrystalline materials, whereas grain boundaries are visible along the nanotubes' length, seen in **Figure 4(c)**.

We examined the crystallinity of the EuS nanotubes via powder x-ray diffraction (XRD) and selected area electron diffraction (SAED). XRD data were collected using a Scintag X_1 θ/θ automated diffractometer with a Cu target (K_α line of λ_α=1.54 Å). In **Figure 5(a)**, we juxtaposed the primary, secondary and tertiary diffraction peaks of bulk EuS [JCPDS card file: 26-1419] with the XRD spectrum of the nanotube samples. The (1 1 1), (2 0 0), and (2 2 0) planes of the FCC EuS crystal structure were identified in the XRD spectrum,

which correspond to 2θ angles of 25.90º, 29.95º and 42.88º respectively. We anticipated peak broadening due to the nanoscale dimensions of the materials. Analysis of the SAED pattern, displayed in **Figure 5(b)**, appeared to support this assertion. The SAED pattern, inverted for ease of analysis and exhibiting the (000) beam block as a "bright spot" [leftmost portion of the image] indicated diffraction of the following planes in fcc EuS: (2 0 0), (2 2 0), (3 1 1), (2 2 2), and (3 3 1), which corresponded to d-spacings of 2.983 Å, 2.109 Å, 1.800 Å, 1.723 Å, respectively. There was an increase in the breadth of the rings, as compared to bulk EuS. Diffraction patterns associated with the interplanar spacings of fcc EuS were present, but were accompanied by similar diffraction rings with both larger and smaller d-spacings. This evidence lead us believe that other phases of EuS may be present.

Photoluminescence measurements of the nanotubes, using an excitation wavelength of 220 nm, reveal a broad emission feature with a peak at ~334 nm (**Figure 6(b)**), whereas the PL spectrum of bulk EuS exhibited a luminescence peak at 615 nm. The peak visible at ~465 nm is due to remnant alumina in the sample, ambient to the nanotube after liberation from the template. Surprisingly, the EuS nanotubes absorbed in the middle-UV region (300 – 200 nm) and emitted in the near-UV region (400 – 300 nm).

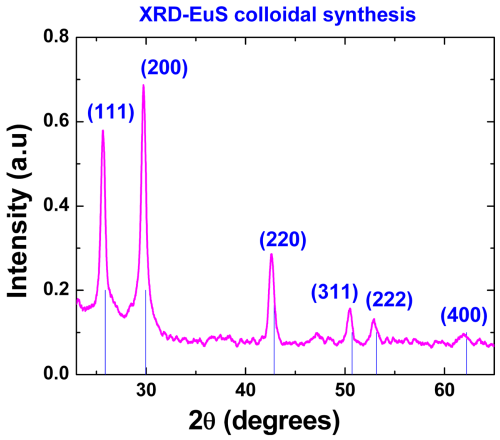

Fig. 7: X-ray diffraction spectrum for colloidally synthesized EuS nanocrystals, approximately 20.0 nm in diameter.

In addition to the typical semiconducting, fcc, NaCl-type (b1) phase, our research offers notable evidence that EuS nanotubes also crystallize in a metallic, simple cubic CsCl-type (B2) phase[13]. The phase transformation from the B2 phase to the B1 phase has been associated with lattice strain[14]. Structural deformations change the crystallinity of the material giving rise to variances in atomic environment; hence, electron exchange interactions. We attribute the strain-induced lattice deformation to the geometry of these nanostructures[15,16]. Lattice deformation in the EuS nanotubes, in part, could have facilitated the blue-shifted optical response observed as a result of crystalline morphing. Further investigations are presently being pursued to define the relationship between lattice deformation, crystallinity and the physical characteristics of EuS nanotubes. Nevertheless, geometric effects were expected to not only influence the optical characteristics of the nanotubes, but also to have given rise to enhanced magneto-optical and magnetic properties as compared to EuS in its bulk and nanocrystal forms. Introducing strain in a crystalline material redefines the structural parameters, which could allow for the manipulation of electron exchange interactions. Further studies are needed to elucidate the effect of strain on the crystallinity and physical properties of europium chalcogenide nanomaterials.

C. Colloidal Synthesis of EuS Nanocrystals:

In parallel to our efforts to synthesize sub-2.0 nm and larger nanocrystals via two-stage, solid state thermolysis techniques[17, 18], which allow us to produce the world's smallest EuS nanocrystals, we are also investigating approaches to produce these materials within the same size regime via colloidal techniques. By producing large quantities of nanocrystals via in solution-phase environments, we afford ourselves additional capabilities to cast these materials into thin films and heterostructures. Such casting abilities significantly increase the feasibility of using the nanocrystals in device applications.[19-21]

Our approach to synthesizing colloidal EuS nanocrystals involved a two-step technique involving precursor precipitation and thermal decomposition of molecular precursors [$Eu(Ddtc)_3(phen)$] in solution using tri-*n*-octylamine, squalene and dimethyl sulfoxide (DMSO) as solvents[2, 3, 22]. Under a nitrogen atmosphere and with vigorous stirring, a 1mM methanolic solution of 1; 10 phenanthroline was added to a 1 mM methanolic solution of europium (II) chloride followed by the addition of a methanolic solution of 2 mM of diethyl ammonium diethyldithiocarbamate producing a lustrous, dark-gray precipitate.

The synthesis was carried out using a standard Schlenk line setup under the flow of argon. To produce EuS nanocrystals, 16 mg of $Eu(Ddtc)_3(phen)$ was mixed with 7 ml tri-*n*-octylamine in a three-neck, round-bottomed flask. This solution was degassed and purged with argon for 15 min at room temperature under continuous stirring. Next, the solution was heated to approximately 100˚C under vacuum and kept at these conditions for 20 minutes. Again the solution was heated to approximately 340˚C at an average rate of 10˚C min^{-1} under a constant argon flow. The solution was maintained at this temperature for 15 min. Upon completion of the refluxing stage, the solution was cooled rapidly to room temperature using a burst of compressed air. The nanocrystals were precipitated using methanol and were centrifuged. The nanocrystal samples were cleaned in methanol and centrifuged at 3500 rpm for 30 minutes. This cleaning step was repeated 4 times. In this approach, tri-n- octylamine, acting as both the reacting solvent and the stabilizer, was used to avoid aggregation and oxidation of the nanoparticles without application of any other surfactants. This procedure currently produces EuS nanocrystals with a broad size distribution. This polydispersity is a characteristic upon which we are hoping to improve during the upcoming months. An XRD analysis (**Figure 7**) of the EuS nanocrystals confirmed the high crystallinity of the nanomaterial by matching the primary diffraction peaks obtained with those of bulk EuS, which crystallizes in the rock salt crystal structure (JCPDF # 26-1419).

The same procedure was carried out with the squalene-based, precursor solution. Nanocrystal samples were cleaned in acetone and centrifuged at 3500 rpm for 30 minutes. This cleaning step was repeated 4 times. This synthesis appears to produce a more narrow range of nanocrystal sizes compared to using tri-*n*-octylamine as the solvent, but the challenge is in removing remnant squalene material from the sample. Though a low boiling point solvent, DMSO forms a solution when combined with the $Eu(Ddtc)_3(phen)$ precursor. Having a homogeneous mixture facilitates uniform decomposition during thermolysis. The boiling point for DMSO is 189˚C; so, we used 175˚C during the synthesis. Nanocrystal samples were cleaned in methanol and centrifuged at 3500 rpm for 30 minutes. This cleaning step was repeated 4 times. This technique also produces a more narrow range of nanocrystal size in comparison with using tri-*n*-octylamine as the solvent (**Figure 8**). As in the case of the squalene-based synthesis, there is some difficulty in removing traces of the solvent from the sample.

We are working towards a size-controlled synthesis procedure in which the products are monodisperse for a wide range of nanocrystal diameters. We will continue to vary the synthesis parameters until we determine on the appropriate conditions.

D. First Synthesis and Characterization of $Pb_{1-x}Eu_xS$ Nanocrystals:

Ternary solid solutions based on IV-VI compound have been studied for many years, as these materials are useful for diode laser applications and for infrared detectors [23-26]. Substitution of the group IV or group VI elements, by cadmium, germanium or tin, changes the band gap and, thus, adds to the tunability. Partial substitution of Mn or Eu for Pb in lead chalcogenides not only can change the band gap but also can produce a dilute magnetic semicondutor[27].

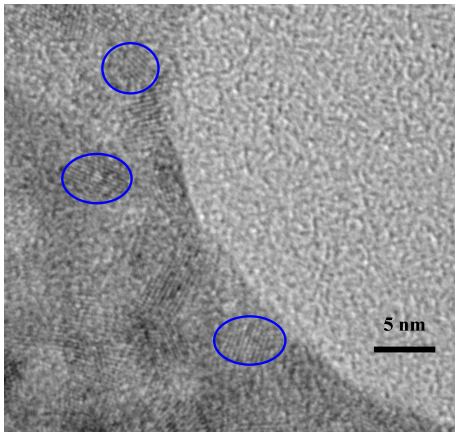

Fig. 8: TEM image of colloidally synthesized, ~5.0 nm EuS nanocrystals in DMSO.

We anticipate that $Pb_{1-x}Eu_xS$ alloys will have a great device potential because of their large stoichiometric tunability. Further, the lattice mismatch between them is only 0.5% [28]. These materials can be tailored to fit plethora of device applications calling for magnetic, semiconducting materials with IR optical characteristics. Ishida et al [28] prepared $Pb_{1-x}Eu_xS$ films for the first time using a hot wall epitaxy technique. However, the nanocrystalline $Pb_{1-x}Eu_xS$ materials have not yet been reported. Nanocrystalline materials are currently being studied extensively to elucidate the relationship between particle size and physical properties originating from quantum confinement effect, large surface-to-volume ratio, and strain at very small sizes. Alloy nanocrystals provide an additional

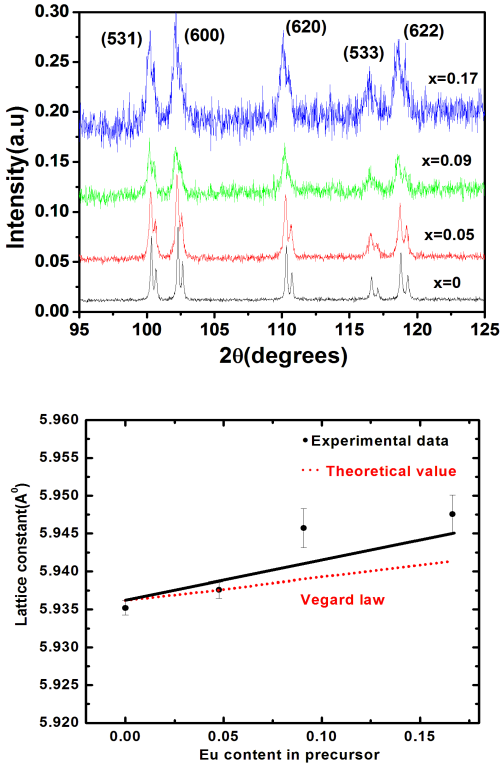

Fig. 9: top) XRD spectra of $Pb_{1-x}Eu_xS$ (x=0, 0.5, 0.09 and 0.17) nanocrystals. bottom) Dependence of the lattice constants of $Pb_{1-x}Eu_xS$ nanocrystals on the EuS precursor content. Dashed line represents Vegard's relation and solid line represents experimental data.

degree of freedom in selecting desirable properties for nanoscale engineering because their physical properties depend on both size and composition. It is likely that nanocrystalline materials of rare earth alloys will exhibit improved magnetic and optical responses.

We have developed the first synthesis of nanocrystalline, alloyed, $Pb_{1-x}Eu_xS$. Although ternary nanocrystals are synthesized by solid-state reaction, solvothermal, thermolysis or hot injection techniques [29], thermal decomposition of single molecular precursors has been proven to be a more effective method to synthesize nanoscale metals/alloys and metallic chalcogenides [1, 30]. The use of a single precursor source is convenient, for alloys; however, this method is limited by the precursor availability and their tedious, yet complicated synthesis procedure [29, 31].

To synthesize $Pb_{1-x}Eu_xS$ ternary alloy nanocrystals, we used a facile, thermolysis technique utilizing mixed precursors of 1,10-phenanthroline, europium diethyldithiocarbamate complex $[Eu(Ddtc)_3(phen)]$ and a 1,10-phenanthroline, lead diethyldithiocarbamate complex $[Pb(Ddtc)_3(phen)]$. A certain molar ratio of these chemicals was dissolved in DMSO, followed by vigorous stirring. The resulting solution was dried using rotary evaporator and then under vacuum. Thermolysis of the resultant precursor at ~ 1hr and 700˚C produced $Pb_{1-x}Eu_xS$ nanocrystals. The [Pb]/[Eu] composition in the alloyed material can be adjusted according to the ratio of precursor used. In this study, we have synthesized $Pb_{1-x}Eu_xS$ nanocrystals with the following EuS precursor content: x = 0, 0.05, 0.07, 0.09, 0.13 and 0.17.

Our assessments of the structure of the $Pb_{1-x}Eu_xS$ nanocrystals involved X-ray diffraction (XRD), Transmission electron microscopy (TEM), and Raman spectroscopy. XRD and TEM measurements assist in the indication of the atomic arrangement (crystallinity) of the nanocrystals. Raman Spectrometry provides information about the structure, composition and lattice dynamics of the surface layer of ternary nanocrystals.

X-ray diffraction (XRD) measurements of our nanocrystals were obtained using a Scintag X_1 θ/θ automated powder diffractometer. **Figure 9 (top)** shows the X-Ray Diffraction pattern of $Pb_{1-x}Eu_xS$ (x=0, 0.05, 0.09 and 0.17) nanocrystals together with the indexing of five higher angle diffraction planes. These traces confirm the formation and composition of the alloys of $Pb_{1-x}Eu_xS$ ternary system. Experimental data shows good agreement with the standard JCPDS data. As the Eu content of the alloyed nanocrystals increases, the diffraction peaks in the XRD patterns gradually shift toward shorter angles. The lattice constant of $Pb_{1-x}Eu_xS$ nanocrystal was deduced from the average shift of diffraction peaks relative to those of PbS. In doing this,

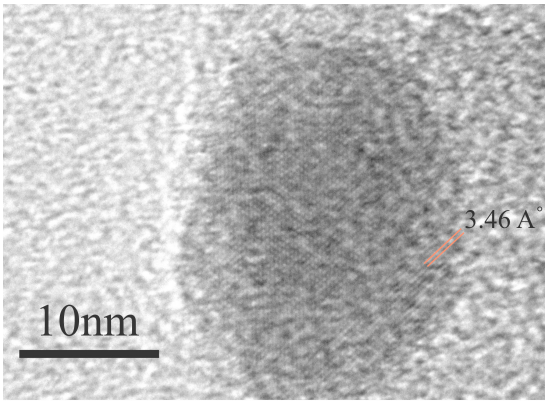

Fig. 10: TEM image of ~ 20nm $Pb_{1-x}Eu_xS$ (x=0.09) nanocrystal.

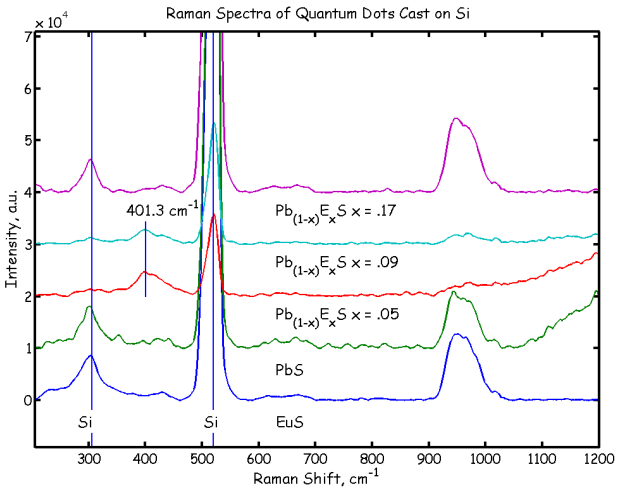

Fig. 11: Raman spectra of the $Pb_{1-x}Eu_xS$ nanocrystals with different Eu compositions.

we used data corresponding to ten higher angle diffraction planes beginning with (5 1 1) and ending with (6 4 0). The results are shown in **Figure 9 (bottom)** and indicate that the lattice constant of $Pb_{1-x}Eu_xS$ nanocrystals is a linear function of EuS content in the precursor. This trend is consistent with Vegard's law (dotted line), which confirms the formation of alloyed nanocrystals with a homogenous distribution of EuS inside the PbS matrix.

For our analysis of the size and structure of the nanomaterials, methanolic solutions of the $Pb_{1-x}Eu_xS$ nanocrystals were dropcasted onto holey carbon films mounted on TEM specimen grid (Ted Pella,Inc.). TEM images were obtained using a Philips CM 20 microscope operating at 200 kV. **Figure 10** shows a TEM image of the synthesized 20 nm $Pb_{1-x}Eu_xS$ (x=0.09) nanomaterial.

Raman scattering measurements were performed in air at room temperature on EuS, PbS, and $Pb_{1-x}Eu_xS$ (x = 0.05, 0.09 and 0.17) nanocrystals, with the focus of the beam of a He-Ne laser (633 nm) via an optical microscope in a backscattering geometry. Raman peak positions for $Pb_{1-x}Eu_xS$ (x = 0.05, and 0.09) nanocrystals clearly differed from those of EuS and PbS nanocrystals.(**Figure 11**). We attribute these shifts of the Raman peaks mainly to the composition change. This indicates the formation of homogenous $Pb_{1-x}Eu_xS$ alloy nanocrystals. For x=0.17 sample, its Raman spectrum presents a two-phase structure (the mixture of pure PbS and EuS nanocrystals). More detailed investigation of the two-phase structure requires a juxtaposition of Raman, XRD, and atomic resolution scanning transmission electron microscopy (Z-STEM), which is the subject of future work.

E. Magnetic characterization of 4nm and 14 nm EuS nanocrystals:

Magnetic measurements on larger EuS nanocrystals (4 nm and 14 nm) were conducted at the National High Magnetic Field Laboratory in Tallahassee, Florida with a Quantum Design 16-Tesla Physical Property Measurement System (PPMS). Key experiments included the zero-field-cooled and field-cooled magnetic moment measurements as functions of temperature, and magnetization hysteresis loop measurements, conducted on powders of the EuS nanocrystals. This would provide additional evidence of the size dependence of the magnetic characteristics.

The magnetization response of 14nm nanocrystal across a temperature range

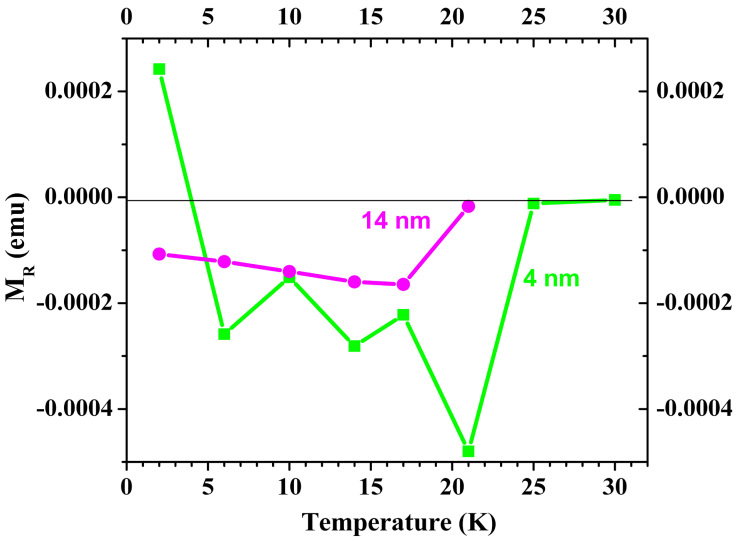

Fig 12: Remnant magnetization (M_R) versus temperature for 4 nm and 14 nm europium sulfide nanocrystals. For the majority of the temperatures, M_R is reversed.

from 2 to 21K was measured. At 2 K, the counterclockwise hysteresis curve, typical for the ferromagnetic materials, was observed. Such a hysteresis yields a positive remanent magnetization (M_R). When the temperature increased, the hysteresis curve reversed direction, becoming clockwise. M_R measurements performed on 4 nm EuS nanocrystals are comparable to previously reported measurements in which a reversal in M_R was observed as a function of temperature.[32] Investigation of magnetic properties for 14 nm EuS nanocrystals has shown a similar reversal phenomenon, which was not anticipated. The magnitude of M_R as a function of temperature for both 4nm and 14nm are displayed in **Figure 12**. The data confirmed the magnetization reversal phenomena for 4nm nanocrystals, but revealed a similar phenomenon in larger nanocrystals. We desire to investigate the extend of this reversal as the nanocrystals increase in size up to 20 nm, for which bulk-like traits should dominate.

5. List of Publications Associated with DOE Project:

1. John G. Kelly, Weidong He, Suseela Somarajan, Kevin G. Yager, and James H. Dickerson, *Wide Angle X-Ray Diffraction Studies of Nanocrystalline Lead Europium Sulfide*, Materials Letters 89,198, 2012.
2. S. Somarajan, M. A. Harrison, D. S. Koktysh, W. He, S. A. Hasan, J.-H. Park, R. L. Stillwell, E. A. Payzant, and J. H. Dickerson, *Structural and Magnetic Analysis of Nanocrystalline Lead Europium Sulfide (PbxEuyS),* Materials Chemistry and Physics 134,1-6, 2012.
3. S. Somarajan, A. J. Krejci, W. He, D. S. Koktysh, and J. H. Dickerson, *Concentration dependence of the exchange interaction in lead europium sulfide nanocrystals*, Solid State Communications 152, 161, 2012.
4. W. He and J.H. Dickerson, *Insight into Thermally Driven Isotropic Crystallinity Breaking: The 1D Assembly of Europium Chalcogenide Nanoparticles with Oleate Ligands*, Applied Physics Letters 98, 081914 2011.
5. M.A. Harrison, S. Somarajan, S.V. Mahajan, D.S. Koktysh, K. van Benthem, and J.H. Dickerson,*Template Assisted Synthesis of EuS Nanotubes*, Materials Letters 65, 420, 2011.
6. D.S. Koktysh, S. Somarajan, W. He, M.A. Harrison, S.A. McGill, and J.H. Dickerson, *EuS nanocrystals: a novel synthesis for the generation of monodisperse nanocrystals with size-dependent optical properties*, Nanotechnology 21, 415601, 2010.
7. A.M. Thron, C.S. Bonifacio, N. Erdman, M.A. Harrison, S. Somarajan, J.H. Dickerson, and K. van Benthem, *Characterization of EuS Nanotubes in Quantum Confinement*, Microscopy and Microanalysis 15, 1178, 2009.
8. M.L. Redígolo, D.S. Koktysh, K. van Benthem, S.J. Rosenthal, and J.H. Dickerson, *Europium Sulfide Nanoparticles in the Sub-2nm Size Regime*, Materials Chemistry & Physics 115 (2-3), 526, 2009.
9. S. Somarajan, S.A. Hasan, M.A. Harrison, C.T. Adkins, E. Harth, and J. H. Dickerson, *Electrophoretic Deposition of Star Polymer–Europium Chalcogenide Nanocomposite Films*, Key Engineering Materials **412**, 113, 2009.

6. Personnel:

Graduate Students:

A. Melissa A. Harrison, Ph.D. Materials Science, Full Support (100%)

B. Suseela Somarajan, Ph.D. Physics and Astronomy, Full Support (100%)

7. References:

1. M. A. Malik, P. O'Brien and M. Helliwell, Journal of Materials Chemistry **15** (14), 1463-1467 (2005).
2. F. Zhao and S. Gao, Journal of Materials Chemistry **18** (9), 949-953 (2008).
3. T. Mirkovic, M. A. Hines, P. S. Nair and G. D. Scholes, Chemistry of Materials **17** (13), 3451-3456 (2005).
4. F. Zhao, H. L. Sun, S. Gao and G. Su, Journal of Materials Chemistry **15** (39), 4209-4214 (2005).
5. R. A. Ivanov, I. E. Korsakov, N. P. Kuzmina and A. R. Kaul, Mendeleev Communications (3), 98-99A (2000).
6. M. D. Regulacio, K. Bussmann, B. Lewis and S. L. Stoll, Journal of the American Chemical Society **128**, 11173-11179 (2006).
7. M. D. Regulacio, N. Tomson and S. L. Stoll, Chemistry of Materials **17** (12), 3114-3121 (2005).
8. D. J. Sellmyer, M. Yu and R. D. Kirby, Nanostructured Materials **12** (5-8), 1021-1026 (1999).
9. D. J. Sellmyer, M. Yu, R. A. Thomas, Y. Liu and R. D. Kirby, Physics of Low-Dimensional Structures **1-2**, 155-165 (1998).

10. S. H. Sun and C. B. Murray, Journal of Applied Physics **85** (8), 4325-4330 (1999).
11. K. v. Benthem and S. J. Pennycook, *Electron Microscopy of Nanomaterials at very High Resolution*, Second ed. (Dekker, New York, 2008).
12. F. Zhao, H. L. Sun, G. Su and S. Gao, Small **2** (2), 244 (2006).
13. V. C. Srivasta and R. Stevenson, Canadian Journal of Physics **46** (23), 2703 (1968).
14. I. N. Goncharenko and I. Mirebeau, Physical Review Letters **80** (5), 1082-1085 (1998).
15. C. N. R. Rao, A. Govindaraj, F. L. Deepak, N. A. Gunari and M. Nath, Applied Physics Letters **78** (13), 1853-1855 (2001).
16. Q. Chen, G. H. Du, S. Zhang and L. M. Peng, Acta Crystallographica Section B-Structural Science **58**, 587-593 (2002).
17. M. L. Redigolo, D. S. Koktysh, S. J. Rosenthal, J. H. Dickerson, Z. Gai, L. Gao and J. Shen, Applied Physics Letters **89** (22), 222501 (2006).
18. M. L. Redígolo, D. S. Koktysh, K. van Benthem, S. J. Rosenthal and J. H. Dickerson, Materials Chemistry and Physics **115** (2-3), 526-529 (2009).
19. S. A. Hasan, D. W. Kavich, S. V. Mahajan and J. H. Dickerson, Thin Solid Films **517** (8), 2665-2669 (2009).
20. S. V. Mahajan, S. A. Hasan, J. Cho, M. S. P. Shaffer, A. R. Boccaccini and J. H. Dickerson, Nanotechnology **19** (19) (2008).
21. S. Somarajan, S. A. Hasan, C. T. Adkins, E. Harth and J. H. Dickerson, Journal of Physical Chemistry B **112** (1), 23-28 (2008).
22. S. Thongchant, Y. Hasegawa, Y. Wada and S. Yanagida, Journal of Physical Chemistry B **107** (10), 2193-2196 (2003).
23. A. R. Calawa, Journal of Luminescence **7**, 477-500 (1973).
24. D. L. Partin, Superlattices and Microstructures **1** (2), 131-135 (1985).
25. D. L. Partin, Ieee Journal of Quantum Electronics **24** (8), 1716-1726 (1988).
26. S. P. Zimin, E. A. Bogoyavlenskaya, E. S. Gorlachev, V. V. Naumov, D. S. Zimin, H. Zogg and M. Arnold, Semiconductor Science and Technology **22** (12), 1317-1322 (2007).
27. T. Dietl, Nature Materials **2** (10), 646-648 (2003).
28. A. Ishida, N. Nakahara, T. Okamura, Y. Sase and H. Fujiyasu, Applied Physics Letters **53** (4), 274-275 (1988).
29. D. C. Pan, L. J. An, Z. M. Sun, W. Hou, Y. Yang, Z. Z. Yang and Y. F. Lu, Journal of the American Chemical Society **130** (17), 5620-+ (2008).
30. M. A. Malik, P. O'Brien and M. Helliwell, Journal of Materials Chemistry **15** (14), 1463-1467 (2005).
31. D. Pan, L. An, Z. Sun, W. Hou, Y. Yang, Z. Yang and Y. Lu, J.Am.Chem.Soc. (2008).
32. M. L. Redígolo, D. S. Koktysh, S. J. Rosenthal, J. H. Dickerson, Z. Gai, L. Gao and J. Shen, Applied Physics Letters **89** (22) (2006).